ChemPubSoc Europe

DOI: 10.1002/cphc.201300411

Calibration of the X-Ray Photoelectron Spectroscopy Binding Energy Scale for the Characterization of Heterogeneous Catalysts: Is Everything Really under Control?

Marc Jacquemin,[a] Michel J. Genet,[b] Eric M. Gaigneaux,[a] and Damien P. Debecker*[a]

Investigations of X-ray photoelectron spectra from solid samples need corrections for the surface charging effect. For powder samples such as heterogeneous catalysts and their supports, the **C**–(C,H) component of the C 1s peak is often used as an internal standard for the calibration of the binding energy scale. Although this method is widely recognized as suitable for the study of heterogeneous catalysts, we show that a significant calibration bias can be encountered upon comparing samples with different bulk composition. In this paper, a series of SiO_2–Al_2O_3 supports and Pd/SiO_2–Al_2O_3 catalysts with various Si/Al ratios were studied. The spectra issued from these samples were processed with the classical calibration method on the basis of the carbon peak. Important discrepancies in the relative position of the photoelectron peaks were noticed. After systematically discarding instrument-related issues, a true chemical influence of the bulk matrix on the analyzed surface species was evidenced. The extent of this chemical effect was dependent on the composition of the sample and more precisely on its ionicity. Two possible mechanisms for this chemical effect were proposed and discussed. Finally, an alternative calibration method was offered.

1. Introduction

Heterogeneous catalysis is based on reactions that occur on active sites located at the surface of solids. The study of materials surface is thus essential for the understanding of their properties and for the development of high-performance catalytic materials. In particular, X-ray photoelectron spectroscopy (XPS) is a powerful technique for the identification and quantification of elements that are present at the surface of solids.[1] Determining the XPS binding energy (BE) of peaks characteristic of the catalytically active elements helps to reveal their oxidation state and to correlate this information with the catalytic performance.[2] XPS also helps to describe the dispersion of an active phase on a support. In metal nanoparticle based catalysts, for example, in the case of Pd-based catalysts, the BE of Pd photoelectrons was shown to be linked to the size of the nanoparticle, which itself controls the catalytic activity.[3]

If using XPS, the determination of the exact BE of each recorded peak is thus a crucial step. The analyzer measures the kinetic energy (KE) of the detected electrons and deduces their BE as the difference between the energy provided by X-ray irradiation ($h\nu$) and the KE, corrected by the spectrometer work function (Φ) and the surface charging effect (E_c) [Eq. (1)]. The Φ term represents the work required to bring an electron from zero attraction by the sample (Fermi level) to the entrance of the energy analyzer. This term is constant for a given spectrometer and can be quantified by a specific calibration by using a clean gold sample as a reference.[4] The value of E_c is generated during the analysis: as photoelectrons are ejected, a positive charge builds up at the surface of the sample and shifts the KE scale.

$$\mathrm{BE} = h\nu - \mathrm{KE} - \Phi - E_c \quad (1)$$

As this phenomenon is sample dependent, E_c has to be determined for each sample. Provided this charging reaches a stable value, and with the help of an appropriate reference (see below), a calibration can be applied to correct for the surface charging effect.

One fundamental and practical aspect of XPS that must be predicted, understood, and mastered is the charging effect, especially at the surface of insulating or complex surfaces.[5] First, E_c needs to be stable over the analysis time. Second, it must be the same on the different components of the complex samples. In particular, the positive charge developed at the surface of the sample must be the same as the positive charge on the

[a] Dr. M. Jacquemin, Prof. E. M. Gaigneaux, Dr. D. P. Debecker
Institute of Condensed Matter and Nanosciences (IMCN)
Molecules, Solids and Reactivity (MOST)
Université catholique de Louvain, Croix du Sud 2/L7.05.17
1348 Louvain-la-Neuve (Belgium)
E-mail: damien.debecker@uclouvain.be

[b] M. J. Genet
Institute of Condensed Matter and Nanosciences (IMCN)
Bio- and Soft Matter (BSMA) and
Surface Characterisation Platform (SUCH)
Université catholique de Louvain, Croix du Sud 2/L7.04.01
1348 Louvain-la-Neuve (Belgium)

Supporting information for this article is available on the WWW under http://dx.doi.org/10.1002/cphc.201300411.

component that is used as the standard; otherwise, the calibration will be clearly biased (differential charge). One method to avoid fluctuations and to stabilize this charge over the entire surface of the sample is to send a flow of low-energy electrons to the surface through an electron flood gun or a charge neutralizer. These electrons overcompensate the charging effect by imposing a stable negative potential. The value of E_c, therefore, becomes negative but constant. However, in the case of complex samples containing both insulating and conducting components, this compensation is sometimes not uniform and a differential charge can still be observed.[6] That is, the conducting component gets rid of the negative charge sent to the surface, whereas the insulating component is kept at a more negative potential. To overcome this problem, the sample can be isolated from the earth (by using a ceramic sample holder for example) to impede electron conduction and to ensure that all components of the sample are at the same potential.

If the surface charge is indeed stable and uniform, one can use the known BE of one element to calibrate the whole BE scale. A gold coating is often used to that end, for example, in the study of films. However, this strategy is not convenient in the case of powder samples such as heterogeneous catalysts due to the roughness of the surface of the samples.[6,7] The practical alternative is to use the carbon that is contaminating the surface of all the samples as an internal standard. This carbon overlayer comes from the adsorption of organic compounds from the atmosphere or from the spectrometer vacuum chamber.[7a] It is in intimate contact with the catalyst and is thus considered as a good reference. Generally, the energy scale is calibrated so that the **C**–(C,H) component of the C 1s photopeak is fixed at the widely accepted value of 284.8 eV. In the "heterogeneous catalysis community", this calibration method is reputed as acceptable and has been generalized for many years.[6] It is actually fully relevant if similar samples are analyzed and compared (e.g. the same catalyst after different thermal treatments, similar formulations with or without dopant, nanoparticle-based catalysts with different dispersion values but deposited on the same support, etc.).

However, in the present paper, we show that even under the most controlled and favorable analysis conditions, a bias can be encountered if one uses the contamination carbon as an internal standard for a panel of samples with markedly different bulk compositions.

2. Results and Discussion

Silica–aluminas (SiO_2–Al_2O_3) are highly important as catalyst supports in various industrial processes. SiO_2–Al_2O_3-supported catalysts are used in a broad range of important chemical reactions, including olefin metathesis (MoO_3/SiO_2–Al_2O_3),[8] hydrocracking (Ni–W/SiO_2–Al_2O_3),[9] nitrosation of cyclohexane (Co_3O_4/SiO_2–Al_2O_3),[10] ammoxidation (V_2O_5–MoO_3–P_2O_5/SiO_2–Al_2O_3 or TeO_2/SiO_2–Al_2O_3),[11] and hydrodesulfurization (HDS) of gas oil (Ni–Mo–S/SiO_2–Al_2O_3).[12] Pd/SiO_2–Al_2O_3 formulations are well recognized for hydrogenation reactions[13] and methanol synthesis.[14] Herein, we studied a range of Pd/SiO_2–Al_2O_3 catalysts as representative examples of important catalytic systems. We chose to vary the composition of the silica–alumina matrix, and we discuss the impact of this composition on the issue of XPS BE calibration.

2.1. Experimental Observations and Identification of the Problem

Figure 1a–e present the evolution, as a function of the SiO_2 content, of the binding energies of the C 1s [**C**–(C,H) component], O 1s, Si 2p, Al 2p, and Pd 3d peaks for two spectrometers upon fixing the **C**–(C,H) component of the C 1s peak at 284.8 eV as the BE reference (Figure 1a). Upon increasing the SiO_2 content of the samples, a progressive shift to higher binding energies was observed for the O 1s, Si 2p and Al 2p peaks. The shift was almost linear upon increasing the silica content from 10 to 75%. Pure silica slightly steps out of this trend, with a larger shift. These tendencies were observed for both the bare supports and the catalysts (support + Pd impregnated). The same observation was made for both spectrometers (a Kratos Axis Ultra spectrometer and a SSI X-probe (SSX 100/206) spectrometer ; see experimental section), that is, for both insulated and grounded sample holders. In the series of silica–alumina and Pd/SiO_2–Al_2O_3 samples investigated, with various Si/Al ratios, the Si 2p BE ranges between 102.4 and 104.5 eV, the Al 2p BE ranges between 74.5 and 75.5 eV, and the O 1s BE ranges between 531.5 and 533.5 eV. Thus, the energy gap between the position of the **C**–(C,H) component and the position of the constituent elements of the inorganic substrate varies with the composition of the silica–alumina supports. These shifts can be considered substantial and their origin is far from evident. Note that the Si 2p peak is expected near (103.4 ± 0.2) eV regardless of the composition of the silica-based materials.[15] The Al 2p peak of alumina and silica–alumina is expected near (74.5 ± 0.2) eV.[15a]

A priori, XPS BE shifts for a given element are related to modification of the valence state or to differences in the chemical environment of the element. For Si, Al, and O, only one valence state is expected regardless of the composition of the sample (variation of the Si/Al ratio). The progressive replacement of Si atoms by Al atoms, as the alumina content increases, can be considered as a variation of the chemical environment, which could, in principle, induce BE shifts. For example, marked differences in electronegativity between the constitutive elements of a solid are sometimes responsible for shifts in the BE: a very electronegative element makes its direct neighbor atoms more electron deficient and shifts its BE to higher values. This is not the case here, as the difference in electronegativity between Si (1.90) and Al (1.61) is small. Moreover, in the case of such an effect, the BE of both elements should evolve in opposite directions. As Al is less electronegative than Si, the blending of both oxides should result in a lower BE for Si and a higher BE for Al relative to the BE of the pure oxides. This was not observed here (Figure 1c and d). All three peaks (Al 2p, Si 2p, and O 1s) shift together in the same direction. Thus, the interactions between the Si, Al, and O atoms seem to remain constant if the Si/Al ratio changes. The progressive spread between the position of the **C**–(C,H) component of the

C 1s peak and the positions of the elements of the support reveals a different behavior between C on the one hand and the inorganic matrix on the other hand.

In Pd-based catalysts, the Pd $3d_{5/2}$ BE is about (336.3 ± 0.2) eV, as excepted for Pd/SA100 in which the Pd $3d_{5/2}$ BE is 337.2 eV (Figure 1 e). These values indicate that the oxidation state of palladium is +2,[15a,16] as expected, as the final step of the catalysts synthesis is calcination in air. As such, the XPS results show that the Pd $3d_{5/2}$ BE is rather stable in the series of samples studied, and thus appears to be independent of the composition of the support. One should keep in mind, however, that the size of the Pd particles is highly affected by the composition of the support: Pd is better dispersed if the material contains more Al (Table 1). Thus, the mean particle size (D_p) decreases as the SiO_2 content decreases. No linear correlation between the size of the Pd particle and the specific surface area (SSA) could be established. The XPS results, as they are presented in Figure 1 e [if **C**–(C,H) is used as the reference], indicate that the Pd $3d_{5/2}$ BE is not markedly affected by the mean size of the Pd particles. This is in contradiction with previous litera-

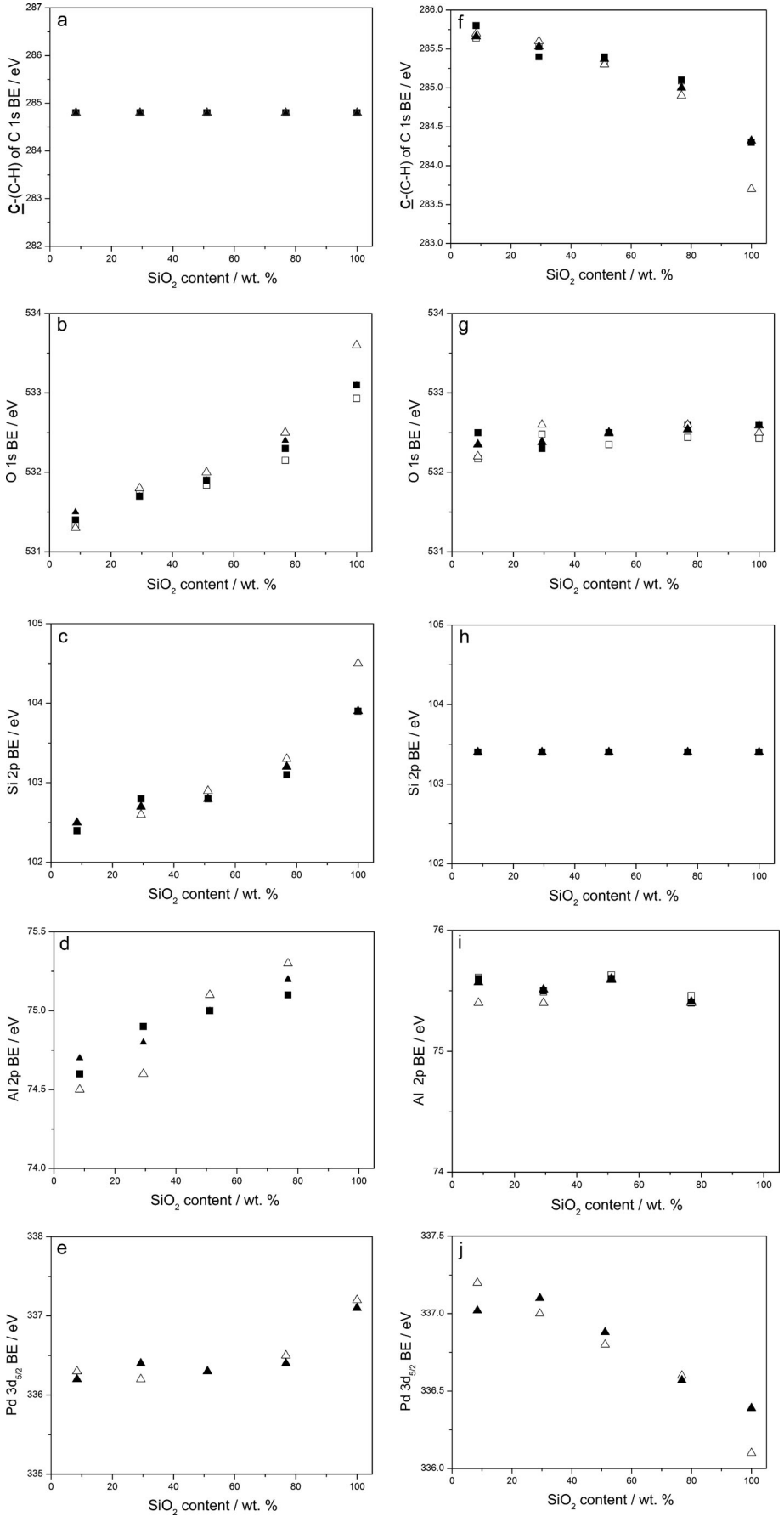

Figure 1. Evolution of the BE of a) the **C**–(C,H) component of the C 1s peak and of the b) O 1s, c) Si 2p, d) Al 2p, and e) Pd $3d_{5/2}$ peaks by using the **C**–(C,H) component of the C 1s peak set at 284.8 eV as the reference for the BE scale. Evolution of the BE of f) the **C**–(C,H) component of the C 1s peak and of the g) O 1s, h) Si 2p, i) Al 2p, and j) Pd $3d_{5/2}$ peaks by using the Si 2p peak set at 103.4 eV as the reference for the BE scale. Open symbols are used for the data recorded with the Kratos spectrometer and the closed symbols are for the data recorded with the SSI spectrometer. (■, □) SA*x* supports; (▲, △) Pd/SA*x* catalysts. The error in the binding energies is around 0.1 eV (see the Supporting Information).

Table 1. Carbon surface concentration of the supports and catalysts measured by XPS with SSI (C_{SSI}) and Kratos (C_{Kr}) spectrometers, SiO_2 at the surface of the supports measured by XPS with the SSI spectrometer, specific surface area (SSA) for the supports measured by N_2 physisorption, and mean size of the palladium particle (D_p) measured by CO chemisorption for the catalysts.

Sample	Support				Catalyst		
	SiO_2 surface [wt%][a]	SSA [$m^2 g^{-1}$]	C_{SSI} [%]	C_{Kr} [%]	C_{SSI} [%]	C_{Kr} [%]	D_p [nm]
SA10	8.5	316	11.6	5.8	10.0	5.0	9
SA30	29.3	340	8.3	9.7	8.8	4.9	13
SA50	51.1	200	5.8	4.1	5.8	3.7	14
SA75	76.7	152	6.3	3.3	4.0	2.7	23
SA100	100.0	429	2.6	1.0	3.7	1.5	27

[a] Deduced from molar elemental concentrations measured with the SSI spectrometer.

Table 2. Charging term calculated and the total photoemitted electron counts for each analysis. The total counts represent the surface under the general spectrum between 0 and 1300 eV.

Sample	SSI spectrometer				Kratos spectrometer			
	Support		Catalyst		Support		Catalyst	
	E_c [eV]	Electron counts	E_c [eV]	Electron counts	E_c [eV]	Electron counts	E_c [eV]	Electron counts
SA10	10.9	1 622 255	10.9	1 236 025	0.9	1 867 457	1.8	1 747 190
SA30	11.1	1 478 571	11.0	1 337 635	1.8	2 200 181	1.6	1 949 879
SA50	11.0	1 298 724	11.0	1 061 600	0.9	2 012 159	2.4	1 641 938
SA75	10.9	1 776 927	10.9	1 123 877	0.8	1 968 924	2.8	1 943 011
SA100	11.1	1 368 826	11.3	1 046 657	1.0	2 589 426	2.4	2 068 792

ture reports that demonstrate the size dependence of the core level BE in Pd and PdO nanoparticles.[3,17]

The SiO_2 content at the surface of the supports was checked by XPS with the SSI spectrometer (Table 1). The surface composition appears very close to the bulk composition.

2.2. Assessment of the Experimental Conditions

2.2.1. Surface Charge Stabilization

During XPS analysis, the sample surface acquires a positive charge as a result of the emission of photoelectrons. To avoid fluctuation of this analysis-induced potential, charge overcompensation is imposed either by a flood gun (SSI instrument) or by a combination of an electron source and a charge-balance plate (Kratos instrument). The sample surface is thereby stabilized at a negative potential. This displaces the whole photoelectron spectrum towards lower binding energies. The difference between the apparent BE observed before calibration (E_b*) and the theoretical BE of a given peak [E_b; for example, 284.8 eV for the **C**–(C,H) component of the C 1s peak] is called the charging term (E_c) [Eq. (2)]:[18]

$$E_c = E_b - E_{b*} \quad (2)$$

Calibration simply consists in shifting back the spectrum so that the reference peak is at its expected position. Clearly, if the charge compensation evolves with time during the analysis of one sample, the calibration will be erroneous, and this typically results in poor spectral resolution and/or peak distortion.[19]

Table 2 presents the values of the charging potential obtained on both spectrometers for all of the samples. The E_c values obtained with the SSI spectrometer are relatively high and are constant from one analysis to the other. Contrarily, the charging effect obtained with the Kratos spectrometer evolves from one sample to the other. The analyses were not conducted at the same time on the Kratos instrument [several months separate the analysis of the supports and the analysis of the catalysts (+SA30)], and we observed that the value of E_c was also dependent on the experimental conditions.

Therefore, on the one hand, the SSI spectrometer provides a set of data with excellent charge compensation that is uniform for all samples. On the other hand, the Kratos spectrometer provides a set of data with variable charge compensation. Actually, this would only cause a problem if E_c varies during the analysis of a given sample, but as long as E_c remains stable during the analysis of one sample, regardless of its value, the calibration procedure should shift the whole spectrum back to its normal position. Indeed, after calibration, both spectrometers provided similar BE values for all elements (Figure 1). Additionally, no peak distortion was observed, and the full width at half maximum (FWHM) values were not affected by variations in E_c. Thus, the charge stabilization was not incriminated in the variable energy gap between the positions of the **C**–(C,H) component of the C 1s peak on the one hand and the Si 2p, Al 2p, and O 1s peaks on the other hand.

2.2.2. Amount of Surface Carbon and Total Count of the Photoemitted Electrons

The concentrations of adventitious carbon on the samples investigated are given in Table 1. These concentrations tend to be higher for measurements performed with the SSI instrument because the depth analyzed was smaller than that in the analyses realized with the Kratos instrument. Indeed, 1) the angle of analyses with respect to the sample normal was higher (55 vs 0°) and 2) the acquisition time was longer for measurements with the SSI spectrometer, and thus the accumulation of contaminants was higher. Table 1 also reveals that the carbon contamination tends to decrease as the silica content increases. This trend is classically observed for silica–alumina. Additionally, the nature of the carbon contamination on

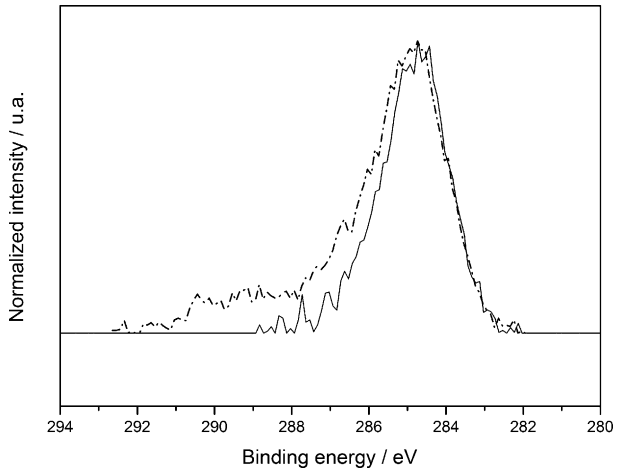

Figure 2. Superposition of the C 1s peaks recorded on SA30 (–•–•) and SA100 (——) supports by using the SSI spectrometer after subtraction of the background. The intensity scale was adjusted so that the peak maxima coincide with each other. The C 1s peaks of SA10, SA30, and SA75 are similar to that of SA50 (see Figure S1 in the Supporting information).

pure silica was slightly different from that on the other supports (Figure 2). The proportion of **C**OO (between 288.8 and 289.3 eV) and **C**–O (286.3 eV) species was lower than that in silica–alumina.[15a]

There, one could see a correlation between the evolution of the C surface concentration and the evolution of the spread between the BE of the **C**–(C,H) component of the C 1s peak and the BE of the constitutive elements of the inorganic substrate (Si 2p, Al 2p, O 1s). Even if both the X-ray energy source and the operating parameters of the charge stabilization devices are maintained constant (which is the case for both spectrometers), the charging term can still be influenced by the total count of the photoelectrons emitted.[20] The latter is logically affected by the thickness of the carbon overlayer. Indeed, the photoelectron cross-section of C is low relative to the photoelectron cross-section of O, which is the main contributor to the total count in such oxides. Thus, the total count obtained from a surface with a thick layer of adventitious carbon is lower than that obtained from a "clean" surface.[21]

However, such correlations between the thickness of the carbon layer and the charging effect have been established for flat surfaces with relatively thick carbon layers. Here, even if the carbon surface concentration is not constant, it remains relatively low. If we consider that the contamination homogeneously covers the sample surface, the thickness of the contamination layer is also low. Consistently, we found no correlation between the C surface concentration and the total photoelectron counts or the charging term (Figure S2–S5 in the Supporting Information). The evolution of the BE of the Si 2p, Al 2p, and O 1s peaks with respect to the position of the C 1s peak is thus not explained by these slight differences in C surface concentrations. It should logically find its explanation in relation with the actual chemical nature of the samples under study.

2.2.3. Effect of the Inorganic Matrix on the Carbon Layer

The only reasonable explanation for the problems outlined above is linked to unreliable energy scale calibration on the basis of the position of the C 1s peak. We suspected that the interactions between adventitious carbon and the substrate on which it is deposited are not constant in the series of silica–alumina-based samples investigated here (Figure 3). These interactions would in turn account for shifts in the actual BE of the carbon atoms. Clearly, upon calibration, all C 1s peaks are set to their "normal" position [i.e. **C**–(C,H) component at 284.8 eV], but the other elements would be shifted relative to their expected positions. Such an effect of the interaction between the sample and the adventitious carbon, which affects

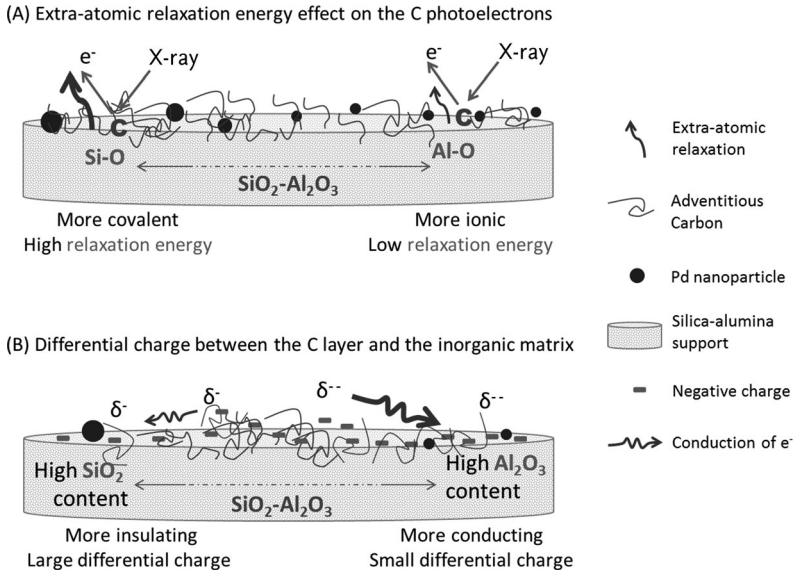

Figure 3. View of the possible effects of the inorganic matrix on the C 1s BE. The scheme depicts the situation for silica-rich samples (left) and for alumina-rich samples (right). a) Effect described by Kohiki and Oki[22a] on the basis of the fact that the inorganic support provides extra-atomic relaxation energy to the photoelectrons emitted from C atoms in adventitious carbon. The energy provided by the more covalent silica-rich supports is higher than the energy provided by the more ionic alumina-rich support. This extra-atomic relaxation energy is symbolized by vertical wave arrows with different sizes and thicknesses. b) Effect based on a differential charging of the adventitious carbon versus the inorganic support. In alumina-rich samples (good conductivity), the adventitious carbon and the inorganic matrix underneath are at the same negative potential (δ^{--}). The large and thick horizontal wave arrow indicates that the electron transfer between surface carbon and the inorganic support is effective. In silica-rich samples (less conducting), the adventitious carbon is maintained at a negative potential (δ^{--}) but the transfer of electron towards the underneath inorganic matrix is less efficient (small and thin horizontal wave arrow) and the latter is thus maintained at a less negative potential (δ^{-}).

the C 1s BE, can be explained in two ways: extra-atomic relaxation energy and differential charging of the carbon contamination.

Extra-Atomic Relaxation Energy[22]

Organic molecules, whether adsorbed on a solid sample or free in the gas phase, can undergo photoemission under the XPS analysis conditions. In the case of adsorbed molecules, however, the BE is lowered by the extra-atomic energy that arises through polarization of the support valence electrons and screen the adsorbate hole state.[22a] This effect is symbolized in Figure 3a. The extra-atomic relaxation mechanism is not the same for ionic and covalent materials. The screening effect in covalent materials is important because the extra-atomic relaxation can take place through the bonds that are polarized. The phenomenon is hampered in ionic materials.[22b,23] Here, if the bulk SiO_2 content increases, the bond ionicity in the samples decreases.[24] Indeed, the Si–O bond is significantly more covalent than the Al–O bond. Thus, if the SiO_2 content increases, ionicity decreases and extra-atomic relaxation takes place more effectively. As a result, photopeaks from adsorbed carbon species are expected at a lower BE.

This effect of the underneath matrix on the superficial carbon is known to be detected only if the carbon layer is thin.[22a] Clearly, if the carbon contamination layer increases in thickness, the intimate interactions between the surface organic carbon atoms and the inorganic matrix are minimized. As discussed above, the concentration of adventitious carbon is low in our study. Consequently, the effect of the inorganic matrix on the surface carbon, as it is explained above, could indeed be invoked to explain the shift between the C 1s peaks and the other photoelectron peaks (Si 2p, Al 2p, O 1s). If one looks at the entire range of silica–alumina series (from 10 to 100% silica), the observed shifts are as large as about 1.5 eV. This variation is substantial and is in the same range as the shifts observed by Opila et al.[22b] for the BE of Si 2p in ZrO_2–SiO_2 and HfO_2–SiO_2 samples. Thus, the phenomena described by Kohiki and Oki[22a] and Opila et al.[22b] could be a first explanation for our observations.

Differential Charging of the Carbon Contamination

Another reasonable explanation that accounts for the differential shifts between Si 2p, Al 2p, and O 1s on the one hand and C 1s on the other hand relies on the presence of a differential charge between the organic contamination overlayer and the support.

The hypothesis is that the interaction between the adventitious carbon overlayer and the inorganic matrix on which it is deposited is not intimate enough to ensure that both are exactly at the same potential. Variations in the ionicity as described above can be extended to variations in the conductivity. Indeed, the transfer of electrons between the organic contamination overlayer and the inorganic sample (see Figure 3b) can be expected to occur more effectively if the Al_2O_3 content increases. This explains the progressive increase in the shifts as the alumina content decreases. For pure silica, a high differential charging effect is present and induces the stepwise BE for this sample (Figure 1, left column).

Such differential charging of the contamination layer relative to the inorganic matrix appears independent of the analysis conditions. It occurs to the same extent if the samples are insulated or grounded, if the charge stabilization is effective or not, and despite the observed small variations of carbon content and total counts of the photoemitted electrons. It is thus clearly a chemical effect linked to the physicochemical properties of the aluminosilicate matrix.

2.2.4. Alternative Calibration Method

In an attempt to describe the surface chemistry of these samples more rigorously, we propose to use a peak of another element belonging to the matrix as a reference for the energy scale calibration. Si atoms in silica–alumina should experience approximately the same environment regardless of the composition of the support.[15] Thus, the Si 2p peak of silicon was chosen as the energy reference. Note that Al 2p could have been chosen as well, as its position evolves in parallel with that of Si 2p.

Figure 1 f–j shows the evolution, with respect to the SiO_2 content, of the BE of the C 1s [**C**–(C,H) component], O 1s, Si 2p, Al 2p, and Pd 3d peaks upon taking the Si 2p peak—fixed at 103.4 eV[15a,c]—as the reference for the calibration of the BE scale.

In this case, the binding energies of the Al 2p and O 1s peaks were not affected by the composition of the samples. This appears more consistent with the fact that the chemical environment of these elements should not vary significantly in the sample panel. Even potential changes in symmetry (octahedral versus tetrahedral coordination) are not expected to yield any shift in the Al 2p BE.[15b] In contrast, as expected, the BE of the **C**–(C,H) component of the C 1s peak (Figure 1 f) decreased if the SiO_2 content was increased, because the conductivity of the substrate decreased.

In parallel, the Pd $3d_{5/2}$ peak shifted progressively to lower BE if the SiO_2 content of the samples was increased. It must be recalled that the mean size of the Pd particle itself increases with the SiO_2 content (Table 1). If one plots the Pd $3d_{5/2}$ BE as a function of the mean size of the palladium particles, a linear relationship is found (Figure 4). The latter is consistent with the results obtained by Wu et al.[3b] on Pd clusters supported on alumina/NiAl(100) materials, by Widjaja et al.[3a] on Pd-based catalysts supported on Al_2O_3/NiO, and by Zhou et al.[3c] on unsupported palladium nanoparticles; all of these results showed that the BE of the Pd nanoparticles decreased as the size of the particle was increased. These previous works were realized either on Pd nanoparticles alone or on Pd nanoparticles supported on a single oxide support. Therefore, energy scale calibration by using the C 1s peak of adventitious carbon was not a problem in those works. In the present case, variations in the support composition were "hiding" the variations in the Pd BE due to a bias in the calibration. Calibration based on the Si 2p photoelectrons allows the link between the size of the Pd

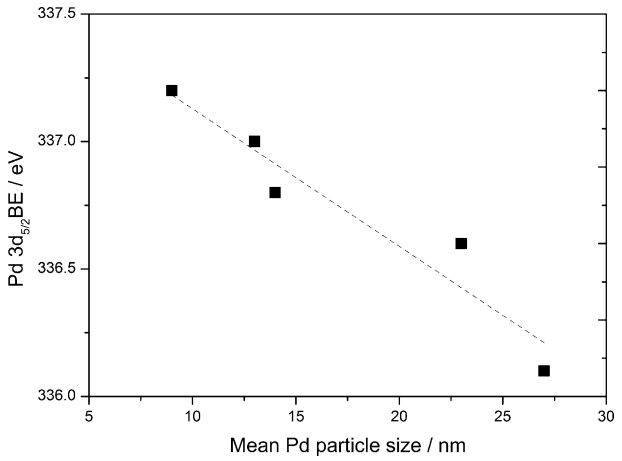

Figure 4. Evolution of the BE of the Pd $3d_{5/2}$ peak as a function of the average size of the Pd particles by using the Si 2p peak set at 103.4 eV as the reference for the BE scale for analyses with a Kratos spectrometer. The error in the Pd $3d_{5/2}$ BE is around 0.1 eV (see the Supporting Information).

nanoparticle and the Pd 3d BE to be highlighted. Importantly, the trend observed in this case is consistent with the confinement effect described by Richter et al.[25]

3. Conclusions

We showed that the composition of the inorganic material analyzed can significantly affect the position of the C 1s peak of the adsorbed carbon species. This influence of the inorganic matrix on the organic layer was shown to be truly linked to the nature of the inorganic material, as technical artifacts were discarded systematically. One explanation calls for the involvement of the extra-atomic relaxation energy from the substrate. The amplitude of this phenomenon is dependent on the ionicity of the substrate, which indeed changes in the series of silica–alumina investigated here. The second reasonable explanation relies on the existence of a differential charge between the inorganic matrix and the carbonaceous layer. The latter, if deposited on a more conducting matrix (alumina-rich) is readily stabilized at the same potential (the electrons are transported effectively from the charge stabilization devices to the carbon layer and to the inorganic substrate). In contrast, as the silica content increases in the substrate, its conductivity drops, and electrons tend to remain on the carbon layer. The latter acquires a lower potential relative to that of the underlying inorganic matrix. A bias is thus introduced in the calibration if the samples are very different from one to another and if the **C**–(C,H) component of the C 1s peak is used as the reference.

Choosing another element that is not expected to be affected by variations in the chemical composition appears more relevant. If the Si 2p peak is used as the reference for the energy scale calibration, a linear relationship between the Pd $3d_{5/2}$ BE and the size of the Pd particles is established, which is in agreement with what would be expected after studies on Pd nanoparticles.

Experimental Section

Materials

The SiO_2–Al_2O_3 supports were synthesized by coprecipitation through hydrolysis of ethyl orthosilicate and aluminum isopropoxide as described by Rouxhet and co-workers.[26] The supports are denoted S*a*x, in which *x* stands for the silica weight content in % and ranges from 10 to 100. Prior to the syntheses of the catalysts, the supports were calcined at 500 °C for 15 h under static air in a muffle furnace.

The Pd/SiO_2–Al_2O_3 catalysts were prepared by using a classical wet impregnation technique. The Pd precursor (0.5212 g), tetraammine palladium chloride monohydrate [$Pd(NH_3)_4Cl_2{\cdot}H_2O$, Aldrich, $\geq$99.99%], was dissolved in distilled water (300 mL). The acidity of this solution was adjusted with ammonia (Fisher Scientific, 35 wt% in solution) up to pH 10.6. The calcined support (4 g) was mixed with the solution for 1 h under magnetic stirring. Water was then evaporated under reduced pressure by using a rotavapor at 40 °C. The recovered solid was dried in air for one night at 110 °C and calcined at 500 °C for 3 h in a muffle furnace under static air. Catalysts are denoted Pd/SA*x*. It should be noted, however, that the palladium phase is in its oxide form (PdO). The palladium loading was 5 wt%.

Basic Characterization

The compositions of the supports and the Pd loadings were verified by using inductively coupled plasma atomic emission spectroscopy (ICP-AES) with an ICAP 6500 Thermo Scientific apparatus.

The dispersion of the Pd particles was determined by carbon monoxide chemisorption. CO chemisorption measurements were conducted at 35 °C after reduction, under an atmosphere of H_2 (Praxair, 99.995%), of the samples during 2 h at 300 °C by using a Micromeritics Pulse Chemisorb 2700 apparatus equipped with a TCD detector. Several pulses of a known volume of CO (185 μL) were admitted sequentially on the samples. The metallic dispersion was calculated from the cumulative amount of adsorbed CO as follows [Eq. (3)]:

$$D = \frac{V_T M}{V_M m C L} \times 100 \quad (3)$$

in which D is the metallic dispersion [%], V_T is the total volume of adsorbed CO under normal temperature and pressure conditions, M is the atomic weight of the metal (i.e. Pd = 106.42 g mol^{-1}), V_M is the molar volume (22.414 L mol^{-1}) of the active gas under normal conditions (0 °C, 101.3 kPa), m is the sample mass, C is the CO adsorption stoichiometry coefficient on Pd (one adsorbed CO molecule per atom of Pd),[27] and L is the wt% of the metal (i.e. Pd) in the sample determined by ICP-AES.

The particle size of the Pd on the catalysts was estimated by the following equation [Eq. (4)]:

$$d = \frac{500M}{\rho \sigma D} \quad (4)$$

in which d is the particle size [m], M is the atomic weight of the metal (i.e. Pd = 106.42 g mol^{-1}), ρ is the density of the metal (i.e. Pd = 12.106 g m^{-3}), σ is the surface occupied by one mole of metal (i.e. Pd = 47 800 m^2 mol^{-1}), and D is the metallic dispersion [%].

N_2 physisorption experiments were conducted at −196 °C with a Micromeritics Tristar 3000 instrument. The samples were outgassed at 150 °C under vacuum (2 Pa). The specific surface area was determined by the BET method in the $0.05 \leq P/P_0 \leq 0.30$ partial pressure range.

X-Ray Photoelectron Spectroscopy

A Kratos Axis Ultra spectrometer (Kratos Analytical, Manchester, UK) and a SSI X-probe (SSX 100/206) spectrometer (Surface Science Instruments, USA) were used for the X-ray photoelectron spectroscopy measurements.

The SSI spectrometer was equipped with a monochromated microfocused Al X-ray source (powered at 20 mA and 10 kV). The sample powders pressed in small stainless steel troughs, 4 mm diameter and 0.5 mm depth, were placed on an insulating homemade ceramic specimen holder. The pressure in the analysis chamber was around 10^{-6} Pa. The angle between the surface normal and the axis of the analyzer lens was 55°. The analyzed area was approximately 1.4 mm^2 and the pass energy was set at 150 eV for the survey scan and at 50 eV for the narrow scans. Under the latter conditions, the full width at half maximum (FWHM) of the Ag $3d_{5/2}$ peak of a clean silver standard sample was about 1.1 eV. A flood gun set at 8 eV and a grounded Ni grid placed 3 mm above the sample surface were used for the charge stabilization.

The Kratos spectrometer was equipped with a monochromated aluminum X-ray source (powered at 10 mA and 15 kV) and an eight channeltrons detector. The sample powders were pressed into small stainless steel troughs mounted on a conductive multispecimen holder. The pressure in the analysis chamber was about 10^{-6} Pa. The angle between the surface normal and the direction of photoelectrons collection was 0°. Analyses were performed in the hybrid lens mode, a combination of magnetic and electrostatic lenses. The analyzed area was about 700×300 μm^2. The pass energy of the hemispherical analyzer was set at 160 eV for the wide scan and 40 eV for the narrow scans. Under the latter conditions, the FWHM of the Ag $3d_{5/2}$ peak of a standard silver sample was about 0.9 eV. Charge stabilization was achieved by using an electron source mounted coaxially to the electrostatic lens column and a charge balance plate used to reflect electrons back towards the sample. The electron source was operated at a bias of −1.1 eV. The charge balance plate was set at −2.9 eV and the filament current at 1.8 A for the supports, except for SA30. For the catalysts and SA30, the filament current was fixed at 2.1 A and the charge balance was fixed at −4.1 eV.

Regardless of the spectrometer used, the following sequence of spectra was performed (the peak between brackets was not recorded for the supports): survey spectrum, C 1s, O 1s, Al 2p, Si 2p, (Pd 3d), and C 1s again to check the charge stability as a function of time and the absence of eventual sample degradation during the analyses. The zero of the KE scale of both spectrometers was set by recording the spectrum of a clean standard gold specimen and fixing the BE of the Au $4f_{7/2}$ peak at 83.96 eV. The linearity of the spectrometer energy scale was also checked and adjusted by recording specific well separated peaks on gold and/or copper. The recommended reference binding energies are reported in an ISO standard procedure.[28]

Spectra were decomposed with the CasaXPS program (Casa Software Ltd., UK) by using a Gaussian/Lorentzian (70/30) product function after subtraction of a linear baseline for the Kratos analyses and by using a Gaussian/Lorentzian ratio of 85:15 and a linear baseline for the SSI analyses. Molar fractions were calculated by using peak areas normalized on the basis of acquisition parameters, sensitivity and transmission factors provided by the manufacturers.

The constraints used for decomposition of the Pd 3d peak were as follows: imposing an area ratio Pd $3d_{5/2}$/Pd $3d_{3/2}$ of 1.5, a difference in the binding energies (Pd $3d_{3/2}$–Pd $3d_{5/2}$) of 5.26 eV, and for the Pd $3d_{5/2}$ and Pd $3d_{3/2}$ peaks the same FWHM.[15a,27a] The constraints used for the decomposition of the C 1s peak is simply to use the same FWHM for the **C**–(C,H), **C**–O, and **C**OO components. A difference of 1.5 eV between the **C**–O and **C**–(C,H) components was imposed.

Acknowledgements

Marc Jacquemin is grateful to the FRIA for a PhD Student position. Damien P. Debecker thanks the FNRS for his postdoctoral researcher position. The FNRS is acknowledged for the acquisition of the XPS equipment. The authors acknowledge the financial support from the "Direction Générale des Technologies, de la Recherche et de l'Energie, Région Wallonne" for the project "WINNOMAT2-HYPHARCO" (Convention number 716677). The authors are grateful to Prof. P. Rouxhet for insightful discussions about the XPS results.

Keywords: calibration · carbon contamination · heterogeneous catalysis · ionicity · X-ray photoelectron spectroscopy

[1] a) F. P. Kerkhof, J. A. Moulijn, *J. Phys. Chem.* **1979**, *83*, 1612–1619; b) A. M. Venezia, *Catal. Today* **2003**, *77*, 359–370; c) R. Wojcieszak, M. J. Genet, P. Eloy, P. Ruiz, E. M. Gaigneaux, *J. Phys. Chem. C* **2010**, *114*, 16677–16684.

[2] Y. Suchorski, B. Munder, S. Becker, L. Rihko-Struckmann, K. Sundmacher, H. Weiss, *Appl. Surf. Sci.* **2007**, *253*, 5904–5909.

[3] a) H. Widjaja, K. Sekizawa, K. Eguchi, H. Arai, *Catal. Today* **1997**, *35*, 197–202; b) T. Wu, W. E. Kaden, W. A. Kunkel, S. L. Anderson, *Surf. Sci.* **2009**, *603*, 2764–2770; c) X. Zhou, W. Xu, G. Liu, D. Panda, P. Chen, *J. Am. Chem. Soc.* **2010**, *132*, 138–146.

[4] B. D. Ratner, D. G. Castner in *Surface Analysis—The Principal Techniques*, Wiley, New York, **1997**, pp. 43–98.

[5] a) H. Ebel, M. F. Ebel, E. Hillbrand, *J. Electron Spectrosc. Relat. Phenom.* **1973**, *2*, 277–287; b) M. F. Ebel, H. Ebel, *J. Electron Spectrosc. Relat. Phenom.* **1974**, *3*, 169–180.

[6] G. Johansson, J. Hedman, A. Berndtsson, M. Klasson, R. Nilsson, *J. Electron Spectrosc. Relat. Phenom.* **1973**, *2*, 295–317.

[7] a) A. Cros, *J. Electron Spectrosc. Relat. Phenom.* **1992**, *59*, 1–14; b) D. Dobler, S. Oswald, K. Wetzig, *Anal. Bioanal. Chem.* **2002**, *374*, 646–649.

[8] a) D. P. Debecker, M. Stoyanova, U. Rodemerck, P. Eloy, A. Leonard, B.-L. Su, E. M. Gaigneaux, *J. Phys. Chem. C* **2010**, *114*, 18664–18673; b) D. P. Debecker, M. Stoyanova, U. Rodemerck, A. Leonard, B.-L. Su, E. M. Gaigneaux, *Catal. Today* **2011**, *169*, 60–68; c) D. P. Debecker, D. Hauwaert, M. Stoyanova, A. Barkschat, U. Rodemerck, E. M. Gaigneaux, *Appl. Catal. A* **2011**, *391*, 78–85.

[9] R. Tiwari, B. S. Rana, R. Kumar, D. Verma, R. Kumar, R. K. Joshi, M. O. Garg, A. K. Sinha, *Catal. Commun.* **2011**, *12*, 559–562.

[10] P. L. Liu, H. Xie, K. Y. You, F. Hao, X. F. Li, H. A. Luo, *Catal. Lett.* **2010**, *136*, 150–154.

[11] a) L. Forni, M. Stanga, *J. Catal.* **1979**, *59*, 148–151; b) S. K. Roy, P. Dutta, L. N. Nandi, S. N. Yadav, T. K. Mondal, S. C. Ray, S. Mitra, P. Samuel, *J. Mol. Catal. A* **2004**, *223*, 211–215.

[12] K. Nakano, W. Pang, J.-K. Lee, J.-I. Park, Y. Seong-Ho, I. Mochida, *Fuel Process. Technol.* **2011**, *92*, 1012–1018.

[13] R. Meléndrez, A. Alarcón, G. Del Angel, R. Gómez, *React. Kinet. Catal. Lett.* **2000**, *70*, 113–118.

[14] S. H. Ali, J. G. Goodwin, *J. Catal.* **1997**, *171*, 333 – 338.
[15] a) J.-F. Moulder, W. F. Stickle, P. E. Sobel, K. D. Bomben, *Handbook of X-ray Photoelectron Spectroscopy*, Perkin Elmer Corporation, Waltham MA, **1992**; b) M. J. Remy, M. J. Genet, G. Poncelet, P. F. Lardinois, P. P. Notte, *J. Phys. Chem.* **1992**, *96*, 2614 – 2617; c) C. Sellmer, R. Prins, N. Kruse, *Catal. Lett.* **1997**, *47*, 83 – 89.
[16] M. C. Militello, S. J. Simko, *Surf. Sci. Spectra* **1994**, *3*, 395 – 401.
[17] L. Chen, A. Yelon, E. Sacher, *J. Phys. Chem. C* **2011**, *115*, 7896 – 7905.
[18] G. Vereecke, P. G. Rouxhet, *Surf. Interface Anal.* **1998**, *26*, 490 – 497.
[19] P. G. Rouxhet, M. J. Genet, *Surf. Interface Anal.* **2011**, *43*, 1453 – 1470.
[20] H. J. Busscher, H. C. Van der Mei, M. J. Genet, J. F. Perdok, P. G. Rouxhet, *Surf. Interface Anal.* **1990**, *15*, 344 – 346.
[21] M. J. Genet, C. C. Dupont-Gillain, P. G. Rouxhet in *Medical Applications of Colloids* (Ed.: E. Matijevic), Springer, New York, **2008**, pp. 177 – 307.
[22] a) S. Kohiki, K. Oki, *J. Electron Spectrosc. Relat. Phenom.* **1984**, *33*, 375 – 380; b) R. L. Opila, G. D. Wilk, M. A. Alam, R. B. van Dover, B. W. Busch, *Appl. Phys. Lett.* **2002**, *81*, 1788 – 1790.
[23] C. S. Fadley, S. B. M. Hagstrom, M. P. Klein, D. A. Shirley, *J. Chem. Phys.* **1968**, *48*, 3779 – 3794.
[24] T. L. Barr, S. Seal, H. He, J. Klinowski, *Vacuum* **1995**, *46*, 1391 – 1395.
[25] B. Richter, H. Kuhlenbeck, H. J. Freund, P. S. Bagus, *Phys. Rev. Lett.* **2004**, *93*, 026805.
[26] a) P. O. Scokart, F. D. Declerk, R. E. Sempels, P. G. Rouxhet, *J. Chem. Soc., Faraday Trans. 1* **1977**, *73*, 359 – 371; b) R. E. Sempels, P. G. Rouxhet, *J. Colloid Interface Sci.* **1976**, *55*, 263 – 273.
[27] a) S. Hermans, C. Diverchy, O. Demoulin, V. Dubois, E. M. Gaigneaux, M. Devillers, *J. Catal.* **2006**, *243*, 239 – 251; b) G. Agostini, R. Pellegrini, G. Leofanti, L. Bertinetti, S. Bertarione, E. Groppo, A. Zecchina, C. Lamberti, *J. Phys. Chem. C* **2009**, *113*, 10485 – 10492.
[28] ISO15472, Surface Chemical Analysis—X-ray Photoelectron Spectrometers—Calibration of Energy Scales, ISO, Geneva, **2001**.

Received: April 25, 2013
Published online on ■■ ■■, 2013

ARTICLES

M. Jacquemin, M. J. Genet,
*E. M. Gaigneaux, D. P. Debecker**

■■ – ■■

Calibration of the X-Ray Photoelectron Spectroscopy Binding Energy Scale for the Characterization of Heterogeneous Catalysts: Is Everything Really under Control?

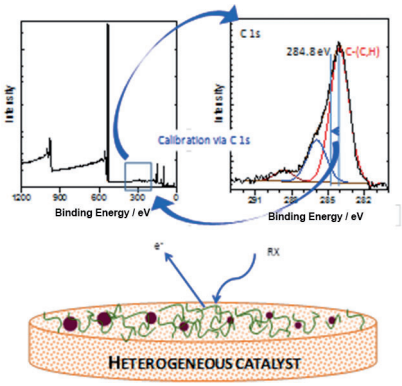

Taking control: X-ray photoelectron spectroscopy (XPS) analysis of heterogeneous catalysts usually relies on binding energy scale calibration by using the C 1s peak as an internal standard. The inorganic solid can, however, have a marked impact on the photoelectron emitted from the adventitious carbon, and this creates an important calibration bias that must be taken into account and corrected for proper use of XPS data.